Mon. Not. R. Astron. Soc. **000**, 1–18 (2013) Printed 2 March 2015 (MN LATEX style file v2.2)

# SPACE WARPS: II. New lens candidates from the CFHTLS discovered through citizen science

Anupreeta More,[1⋆] Aprajita Verma,[2] Phil Marshall,[2,3] Amit Kapadia,[4]
Michael Parrish,[4] Chris Snyder,[4] Julianne Wilcox, Elisabeth Baeten,
Christine Macmillan, Claude Cornen, Surhud More,[1] Raphael Gavazzi,[6] Chris Lintott,[1]
Robert Simpson,[1] David Miller,[3] Arfon Smith,[3] Edward Paget,[3]
Prasenjit Saha,[4] Rafael Kueng,[4] Kelly Borden,[3] Tom Collett,
Thomas Jennings, Matthias Tecza,[1] Layne Wright and possibly others

[1] *Kavli IPMU (WPI), University of Tokyo, 5-1-5 Kashiwanoha, Kashiwa 277-8583, Japan*
[2] *Dept. of Physics, University of Oxford, Keble Road, Oxford, OX1 3RH, UK*
[3] *Kavli Institute for Particle Astrophysics and Cosmology, Stanford University, 452 Lomita Mall, Stanford, CA 94035, USA*
[4] *Adler Planetarium, Chicago, IL, USA*
[5] *Department of Physics, University of Zurich, Switzerland*
[6] *Institut dAstrophysique de Paris, UMR7095 CNRS Université Pierre et Marie Curie, 98bis bd Arago, 75014 Paris, France*

to be submitted to MNRAS

**ABSTRACT**

The CFHT Legacy Survey has been searched for strong lenses with semi-automated algorithms both at galaxy and groups scales. With the aim of improving these lens finding robots, we carry out a blind lens search in the complete CFHTLS WIDE survey with SPACE WARPS. We describe the training sample used for both training the citizen scientists that participated in SPACE WARPS and calibrating their performance. We generate realistic looking simulated samples of lenses both at galaxy and group-scales as part of this training sample. We present 61 new strong gravitational lens candidates discovered from the SPACE WARPS-CFHTLS search out of which 40 candidates are promising. Furthermore, we compile a sample of false positives which can be used for robot testing, first of its kind for the lensing community. The simulated sample is also used to make a comparison between human performance against the robots. We find that the XX per cent of the known lens sample is recovered and the new lens sample has XX completeness with respect to the simulated sample. We make available the following data products: simulated sample, simulation code and the false positives sample at XXX.

**Key words:** gravitational lensing – methods: statistical – methods: citizen science

## 1 INTRODUCTION

The last few decades have seen a rise in the discoveries of strong gravitational lenses owing to the plethora of interesting applications they have in astrophysics and cosmology. Strong lenses are routinely used to probe the dark matter distribution from galaxy (ref) to cluster scales (ref), to study distant young galaxies by using the lensing magnification as a natural telescope (ref), to test the cosmological model by constraining cosmological parameters such as the Hubble constant (ref) and dark energy (ref) and many more. Even though strong lenses are rare, since a foreground massive object needs to be sufficiently aligned with a distant background source to produce multiple images, systematic lens searches have led to discovery of over 500 lenses till date (XXX add mld url).

Rarity of lenses implies searching for them is a painstaking task. Efficient automated methods are thus imperative

⋆ anupreeta.more@ipmu.jp

to finding a reasonably complete and pure sample of strong lenses.

Since the inception of the first citizen science project, Galaxy Zoo, to classify galaxy morphologies (Lintott et al. 2008), several astronomy and non-astronomy projects have been launched by the Zooniverse leading to many interesting project. For example, PlanetHunters has discovered XXX transiting exoplanets (Schwamb et al. 2012), Supernova XXX add ref and XXX add ref

In Paper I, we describe Space Warps, an online system that enables crowd-sourced detection of gravitational lenses. In this paper (referred to as Paper II), we describe our first lens search with Space Warps in the CFHTLS data.

This paper is organised as follows. In Section **??** we give a brief overview of the Space Warps system, focusing on the aspects most relevant to the interpretation of the results of this first lens search. In Section 2 we introduce the CFHTLS imaging data and the known lens samples from the CFHTLS. In Section **??**, we explain the training sample generated to aid the Space Warps users in the lens search. In Section 5, we present the new lens candidates and our findings. We discuss the implications of our results for future lens searches in Section 6 and draw conclusions in Section 7.

## 2 DATA

### 2.1 The CFHT Legacy Survey

The Canada-France-Hawaii Telescope Legacy Survey (CFHTLS) is a photometric survey in five optical bands ($u^*g'r'i'z'$) carried out with the wide-field imager MegaPrime which has a 1 deg$^2$ field-of-view and a pixel size of 0.186″. The CFHTLS WIDE covers a total area of 171 deg$^2$ on the sky and it consists of four fields W1, W2, W3 and W4. The field W1 has the largest sky coverage of 63.65 deg$^2$. The fields W2 and W4 have similar sky coverages of 20.32 deg$^2$ and 20.02 deg$^2$, respectively[1]. The field W3 has a sky coverage of 42.87 deg$^2$ and is more than twice as large as W2 and W4.

The CFHTLS imaging is very homogeneous and has great image quality. Most of the lensed arcs are much brighter in the $g$ band thus, deep imaging in this band is desirable. The limiting magnitude is 25.47 for the $g$ band which goes the deepest among all of the five bands. The mean seeing in the $g$ band is 0.78″. The zero point to convert flux to AB magnitude for all bands is 30. These characteristics make CFHTLS ideal to do visual inspection for finding lenses. We use the data from the final T0007 release taken from the Terapix website[2] for this work.

We note that the CFHTLS is a niche survey with a unique combination of wide imaging with deep sensitivity. It is a precursor to the ongoing wide imaging surveys such as the DES, KIDS and HSC and planned surveys such as the LSST. Searching for lenses with Space Warps in the CFHTLS will teach us important lessons and help prepare us for these larger imaging surveys.

[1] These numbers are estimated from http://terapix.iap.fr/cplt/table_syn_T0006.html
[2] http://terapix.iap.fr/cplt/T0006-doc.pdf

### 2.2 Image Presentation in Space Warps

Our aim is to do a blind lens search over the entire CFHTLS WIDE. We use the $g$, $r$ and $i$-band color imaging which are most useful for visual identification of lenses (and provide access to the $u$ and $z$ band imaging through dashboard with additional tools XXX).

We make color composite images using publically-available code[3] following the prescription of Lupton et al. (2004). Specifically, we first rescale the pixel values of each channel image into flux units, and then apply an arcsinh stretch. The stretch parameters are chosen using a small random sample of images, to ensure that the background noise is just visible, and that the centres of bright, intermediate resdhift galaxies are not saturated. The color scales are chosen to maximize the contrast between faint extended objects. These parameters are then fixed during the production of all the tiles, in order to allow straightforward comparison between one image and another, and for intuition to be built up about the appearance of stars and galaxies across the survey.

We extract contiguous cutouts of size 81.84″ (440 pixels) with an overlapping region of 10″(54 pixels) between the neighbouring cutouts resulting into $\sim$ 430 000 cutouts for the entire CFHTLS WIDE. The size of the individual cutout is determined by optimising factors such as the typical angular scales of gravitational lenses, the number of objects seen in a single cutout and the total number of image cutouts in the survey. It is possible that a lens candidate happens to be too close to the edge of a cutout, the overlap between neighbouring cutout allows the inspector to get a clearer view of the same candidate in at least one of the cutouts. We note that since the images are shown randomly, an inspector may not necessarily come across the neighbouring cutout unless the inspector classifies a large number of images. This is not a problem since our user base is extremely large and we receive multiple classifications of the same cutout.

### 2.3 Existing CFHTLS lens samples

The CFHTLS data has been searched for lenses using semi-automated algorithms, primarily, in the $g$ band where the predominantly faint blue source galaxies are bright compared to the predominantly red deflector galaxies. Here, we briefly mention the lens samples which were known to the authors prior to the lens search with Space Warps.

At galaxy-scales, we focus on two primary lens searches. The RingFinder (Gavazzi et al. 2014) was used for finding compact rings or arcs around centers of isolated and massive early-type galaxies. By subtracting the PSF-matched $i$-band images from the $g$-band images, the algorithm looks for excess flux in the bluer $g$-band. An object detector measures the properties of these residual blue features, and candidates meeting length-width ratio and tangential alignment criteria are then visually inspected to form the final sample. Gavazzi et al. (2014) first selected some 638,000 targets as either photometrically-classified early type galaxies, or objects selected to have red centers and blue outer parts, from the T06

[3] The open source color image composition code used in this work is available from `http://github.com/drphilmarshall/HumVI`

CFHTLS data release catalogs. 14370 were found to show detectable blue residuals, and 2524 were visually inspected, having passed the automatic feature selection process. This led to a sample of 42 good quality (`q_flag` = 3) and 288 medium quality (`q_flag` = 2) lens candidates. In addition to this well defined sample, Gavazzi et al. (2014) reported a further 71 serendipitously detected lens candidates. From this sample of "RINGFINDER candidates," the SL2S team found, during their follow-up campaign, 39 confirmed lenses (and 17 promising candidates). We use this sample of 39 "confirmed RINGFINDER lenses" in our completeness analysis.

The second galaxy-scale lens search was to find edge-on galaxy lenses in the CFHTLS (Sygnet et al. 2010) by selecting the galaxy's profile from the output of SEXTRACTOR in the $i$ band and with low inclination angle. This sample has about 3 promising and a total of 18 lens candidates.

On the other hand, the ARCFINDER More et al. (2012) was used for finding blue arc-like features in the complete CFHTLS data withouth any pre-selection on the type of the lensing object. The search was carried out in the g-band which is the most efficient wavelength to find typical lensing galaxies. This sample, called the SARCS, has 55 promising and a total of 127 lens candidates and consists of both galaxy and groups/cluster scale lens candidates. Arc finding is better suited for lensed images or arcs with larger image separations i.e. more massive systems like groups and clusters. Thus, the SARCS sample has mostly groups/cluster-scale lenses and a few galaxy-scale lenses.

For the purposes of transparency and to help a little with their training, the volunteers participating in SPACE WARPS-CFHTLS lens search were made aware of these known lens samples. Images containing the systems from the above samples were labelled as "Known Lens Candidates" in the Talk forum, where volunteers have the opportunity to discuss their findings with other volunteers and the science team.

## 3 TRAINING SAMPLE: SIMULATED LENSES

*State the importance*

### 3.1 Methodology

We create two main types of simulated lens sample a) galaxy-scale lenses and b) group or cluster-scale lenses. The galaxy-scale lenses are further divided into two types based on the nature of the background sources, namely, galaxies and quasars. Below, we describe how each type of the lens sample was generated.

#### *3.1.1 Galaxy-scale lenses*

The $N_{\rm src}$ behind a lens is then calculated by doing the following integral,

$$N_{\rm src} = N_{\rm src}(> L_s, z_s) \int_{z_l}^{\infty} \sigma_{\rm lens}(\sigma, z_l, z_s, q) D_s^2 (1+z_s)^2 \frac{{\rm d}\chi}{{\rm d}z_s} {\rm d}z_s \quad (1)$$

$$N_{\rm src}(> L_s, z_s) = \int_{L_{min}}^{\infty} \Phi(L_s, z_s) {\rm d}L_s \quad (2)$$

where $\Phi(L_s, z_s)$ is the source luminosity function per unit comoving volume, $q$ is the projected axis ratio of the lens ellipticity, $\chi$ and $D_s$ are the comoving and angular diameter distances to the source,

We use the elliptical galaxy (LRG) catalog from the CFHTLS XXX to select all the foreground galaxies (e.g. $z < 1$) that are potential lenses for the simulated sample. We exclude all those galaxies whose positions match with the lensing galaxies from the known CFHTLS SL2S lens samples More et al. (2012) within 2 arcsec (XXX check).

First, we calculate the luminosity and velocity dispersion of each potential lensing galaxy using the CFHT Megacam $g$ and $r$ band magnitudes along with the photometric redshift ($z_l$) from the LRG catalog. The Megacam magnitudes are converted to SDSS magnitudes[4] and are further k-corrected to redshift $z = 0.1$ (Frei & Gunn 1994). We assume that the evolution of galaxy luminosities is similar to that determined by (Faber et al. 2007), that is, a decline of 1.5 in the $m_{r*}$ from redshift $z = 1$ to $z = 0$ (see Eq. 4).

$$\frac{L}{L_*} = 10.0^{-0.4\ (m_{r\rm SDSS} - m_{r*})} \quad (3)$$

where $m_{r*}$ is

$$m_{r*} = -20.44 + 1.5\ (z_l - 0.1)\,. \quad (4)$$

We use the $L - \sigma$ relation from (Parker et al. 2005) to get the velocity dispersion as given in Eq. 5.

$$\sigma = 142 \left(\frac{L}{L_*}\right)^{1/3} \quad (5)$$

Next, in order to decide whether a galaxy is likely to act as a strong lens, we calculate the lens cross-section ($\sigma_{\rm lens}$) and the number of sources ($N_{\rm src}$) that are in the background. Following (**?**), the lens cross-section is calculated analytically for an isothermal model and is given by

$$\sigma_{\rm lens} = b_I^2 \int_0^{2\pi} 0.5 r^2(\theta) d\theta \quad (6)$$

where $b_I$ is

$$b_I = b_{\rm SIS} \epsilon_3 / sin^{-1}(\epsilon_3)\,, \quad (7)$$

the eccentricity ($\epsilon_3$) is

$$\epsilon_3 = (1 - q_3^2)^{1/2} \quad (8)$$

and the projected axis ratio is given by

$$q_k = \sqrt{q_3^2 {\rm sin}^2 i_e + {\rm cos}^2 i_e}\,. \quad (9)$$

In the above equations, $q_3$ is the 3d axis ratio of the ellipsoid and $i_e$ is the inclination angle. Also, $b_{\rm SIS} = 4\pi \frac{c^2}{\sigma^2} \frac{D_s}{D_{ls} D_l}$ and is referred to as the Einstein radius where

[4] http://www3.cadc-ccda.hia-iha.nrc-cnrc.gc.ca/megapipe/docs/filters.html


**Figure 1.** Examples of the three types of simulated lenses.

$D_s$,$D_l$ and $D_{ls}$ are angular diameter distances to the source, the lens and between the lens and source, respectively.

Next, if the foreground galaxy can act as a lens and has at least one source in the background, then we determine a redshift ($z_s$) and $i$-band magnitude of the background source(s). We assume two types of background sources namely, galaxies and quasars. For each source, the redshift and magnitude are generated by drawing randomly from the following redshift and luminosity distributions. For galaxies, we assume the redshift distribution is

$$p_s = \frac{\beta z_s^2 \exp(\frac{z_s}{z_0(m_{\rm lim})})^\beta}{\Gamma(3/\beta) z_0^3(m_{\rm lim})} \tag{10}$$

where $\beta = 3/2$ and $z_0(m_{\rm lim}) = 0.13 m_{\rm lim} - 2.2$ and the luminosity function is

$$n_s = \int_{-\infty}^{m_{\rm lim}} \frac{n_0 {\rm d}m}{\sqrt{10^{2a(m_1-m)} + 10^{2b(m_1-m)}}} \tag{11}$$

with parameters $a = 0.30$, $b = 0.56$, $m_1 = 20$ and $n_0 = 3 \times 10^3\ deg^{-2}$ as given in (Faure et al. 2009) and references therein. For quasars, we calculate the luminosity function by following the prescription of (**?**) and use k-corrections by (Richards et al. 2006).

The luminosity function is expressed as

$$\frac{{\rm d}\Phi}{{\rm d}M} = \frac{\Phi_*}{10^{0.4(\alpha+1)(M_{\rm abs}-M_*)} + 10^{0.4(\beta+1)(M_{\rm abs}-M_*)}} \tag{12}$$

where the normalization, $\phi_* = 5.34 \times 10^{-6} h^3$ Mpc$^{-3}$ and break magnitude, $M_* = -20.90 + 5{\rm log}h - 2.5{\rm log}f(z)$. The redshift dependent factor in $M_*$ is given by

$$f(z) = \frac{e^{\zeta z_s}(1 + e^{\xi z_*})}{(\sqrt{e^{\xi z_s}} + \sqrt{e^{\xi z_*}})^2}\,. \tag{13}$$

We adopt the best-fit values $\zeta = 2.98$, $\xi = 4.05$, $z_* = 1.60$ (Oguri & Marshall 2010). For the faint end slope, we use $\beta = -1.45$ whereas for the bright end slope, we use $\alpha = -3.31$ when $z_s < 3$ and $\alpha = -2.58$ at higher redshifts, as prescribed by (Oguri & Marshall 2010). respectively. We note that when calculating $N_{\rm src}$, the source number density is artificially boosted by a factor (see Table 1) to increase the occurrence of simulated lenses. This helps in creating a large enough sample to carry out various performance tests.

Next, we determine properties of the background source for every lens. We follow similar procedures for both background galaxies and quasars. For simplicity, we simulate a single background source behind every lens. In order to select one background source from the $N_{\rm src}$ per lens, we do ray-tracing for all of the $N_{\rm src}$ sources with GRAVLENS (Keeton et al. 2000) and choose sources that satisfy criteria as given below. We determine fluxes of the lensed images and the total magnification of each of the lensed source. We draw a random source for which the flux of the second brightest lensed image and the total magnification of all lensed images are above the thresholds given in Table 1.

Since we want to produce realistic looking lens systems, we simulate lenses in each of the five CFHTLS filters. The colors of the background galaxies are drawn randomly from the photometric CFHTLenS catalog (Hildebrandt et al. 2012; Erben et al. 2013). Similarly, we use a quasar catalog from the SDSS Data Release 9 (Pâris et al. 2012) from which colors are drawn to simulate quasar lenses. Next, we assume deVaucoleur's profile to account for the size and shape of the galaxies. The ellipticity and the position angle are drawn randomly between the range given in Table 1. The effective radius of the galaxy is estimated from the Luminosity−size relation (Bernardi et al. 2003) given by

$$R_{\rm eff} = 10^{0.52} \frac{L_r^{2/3}}{(1+z_s)^2} \tag{14}$$

where $L_r = L_s/10^{10.2}$. On the other hand, quasars are assumed to follow a Gaussian profile where the $\sigma$ is equated to that of the median seeing for every filter. The median seeing values are taken from Table 4 of the official Terapix T0007 release explanatory document [5].

Once all the parameters are determined for the lens and source models, GRAVLENS is used to simulate lensed images. After accounting for the shot noise in the lensed images and convolving them with the median seeing in each of the filters, the simulated image is added to the real CFHTLS image centered on the lensing galaxy. Note that we ensure that the lensed galaxies and lensed quasars do not have the same lensing galaxy in the foreground. Similarly, the lensing galaxies from the galaxy-scale lenses are distinct from the central galaxies of groups-scale lenses which are described in the following section.

[5] http://terapix.iap.fr/cplt/T0007/doc/T0007-doc.pdf

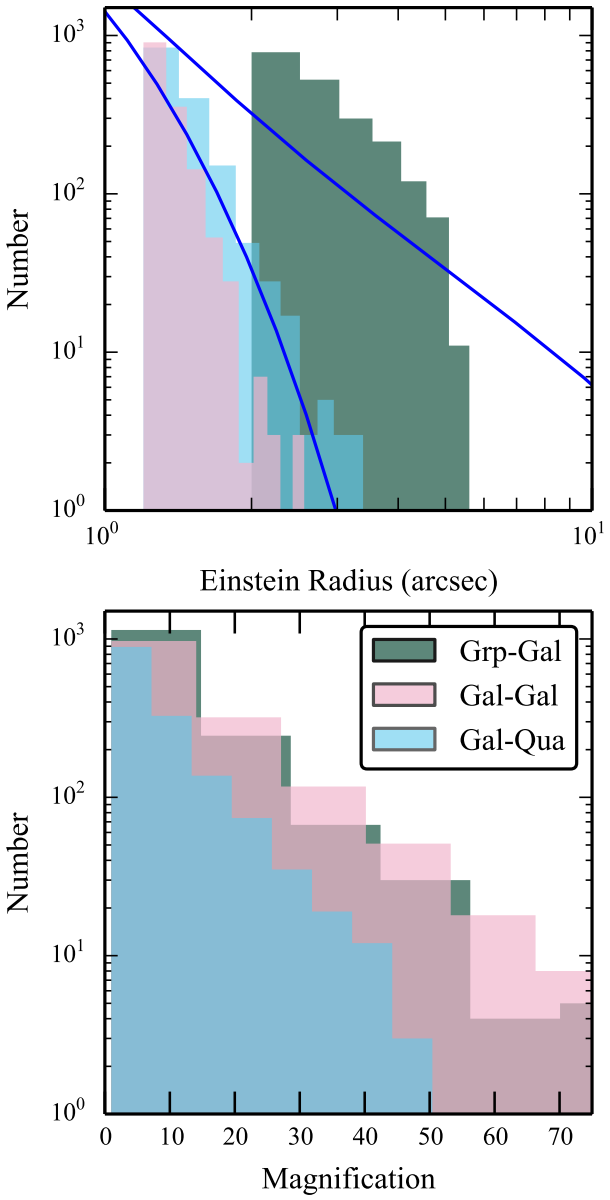


**Figure 2.** Einstein radius distribution for all types of lenses. The dashed-dotted (blue) curves show the theoretical prediction assuming an SIS model at galaxy-scales and a total (NFW+Hernquist) model at groups-scales taken from (More et al. 2012).

### *3.1.2 Groups-scale lenses*

At group or cluster-scales, the brightest group galaxy (BGG) at the center alone does not cause strong lensing. We need to account for the extra convergence arising from the dark matter component as well as satellite galaxies, at least, in the inner regions which are typically responsible for the multiple lensed images (**?**Oguri 2006). Owing to the lack of an appropriate group catalog for our purposes, we create a basic group catalog based on the magnitudes and photometric redshifts available for the CFHTLS. We select all galaxies with $10^{10.8} M_{\odot}$ as the BGGs. We select the member galaxies

**Table 1.** Thresholds used in the selection of the simulated lenses.

| Name | gal | | qso | |
|---|---|---|---|---|
| | min | max | min | max |
| Source Redshift | 1.0 | 4.0 | 1.0 | 5.9 |
| Source Magnitude | 21.0 | 25.5 | 21.0 | 25.5 |
| boost factor | 100 (40†) | | 1200 | |
| Second brightest image | 23 | | 23 | |
| Total magnification | 19 | | 20 | |
| Lens shear strength | 0.001 | 0.02 | 0.001 | 0.02 |
| Lens shear pa | 0 | 180 | 0 | 180 |
| Source ellipticity | 0.1 | 0.6 | | |
| Source PA | 0 | 180 | | |

† – corresponds to the factor used for Groups scale lenses.

such that their photometric redshifts are within $\delta z = 0.01$ of the BGG and within an aperture of 250 Kpc.

We adopt an isothermal ellipsoid for the BGG and members whenever the ellipticities are available else we use an isothermal sphere. On the other hand, we adopt an NFW profile for the underlying dark matter halo. Assuming a constant mass-to-light ratio of $3 \times 0.7$ h $M_*/L_*$, we use the BGG luminosity to estimate the stellar mass. The stellar mass−halo mass relation (**?**), including random scatter, is then used to calculate the halo mass for the lens. Given the halo mass, other key parameters such as the scale radius ($r_s$) and the density at the scale radius ($\rho_s$) can be determined for an NFW profile.

As described in Section 3.1.1, we calculate the luminosity and velocity dispersion for the BGG and each of the member galaxies. Next, we calculate the lens cross-section for each potential lensing group. The complexity in the lens models makes it analytically intractable to calculate the size of the caustics[6]. Hence, we use GRAVLENS to determine the area covered by the caustics. We consider only galaxies as our background source population since group or cluster-scale quasar lenses are not expected to be found in the CFHTLS (check XXX). Following the same procedure as described in Section 3.1.1, we calculate the number of galaxies expected to lie behind every potential lensing group (see Eq. 1). As before, for each background galaxy within the lens cross-section, a redshift and an $i$-band magnitude is determined by drawing galaxies randomly from the respective distributions (see Eqs. 10-11).

All those groups that are found to have no background galaxies within the cross-sectional area are rejected and the rest are included as potential lenses. As mentioned earlier, we artificially boost the total number of sources behind every lens but ensure that (check XXX) the statistical properties such as the profile of the image separation distribution are not affected (see Figure 2). We follow the same procedure and apply the same thresholds to determine properties of the lensed galaxies for every lens as are described for galaxy-galaxy lenses in the previous section. The simulated images

[6] The lens mass distribution determines size and shape of the caustics. Any source located within the caustics will form multiple lensed images which is the criteria for strong lensing. To further understand caustics, see XXX.

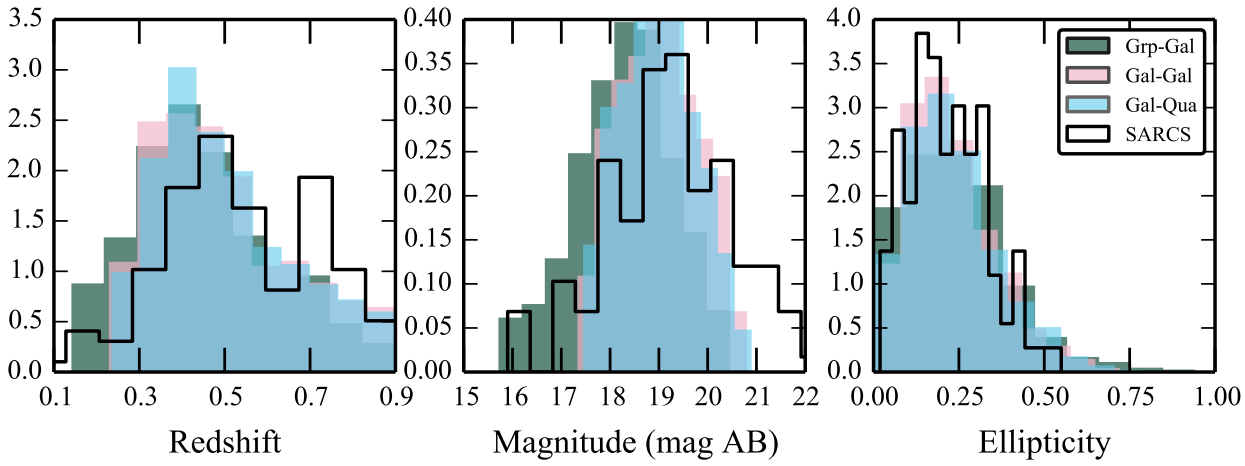


**Figure 3.** Distributions of properties of the lensing galaxies of the simulated sample compared to the known lens sample SARCS XXXX check?

are added to the real CFHTLS images with the BGGs as the center.

### 3.2 Simulated Lens Sample and Catalog Description

In this section, we describe some of the properties of our simulated sample for each of the three types of lens samples.

The Figure 2 shows Einstein radius distribution for the galaxy-scale (dashed for background quasars and dotted for background galaxies) and groups-scale simulated lenses. For comparison, we show the expected distributions (blue dashed-dotted curves) for an SIS-like density profile at galaxy-scales and an NFW+Hernquist profile at groups-scales. The theoretical curves are taken from (More et al. 2012) wherein the models are explained in detail. We note that the model we adopt at groups-scale also includes SIS or SIE components for the group members unlike the theoretical prediction. The theoretical curves have arbitrary normalizations.

We show the redshift and magnitude distributions of the lensing galaxies in the left and right panels of Figure 3 respectively. Furthermore, we overplot the distributions of respective properties of the SARCS lenses from (More et al. 2012) for comparison with arbitrary normalizations. We note qualitative similarities between the simulated and the real lens samples.

Similarly, we show the ellipticity and the position angle of the simulated lens galaxy population extracted from the T0007 release of the CFHTLS catalogs in the left and right panels of Figure 3, respectively. As before, the dashed-dotted (blue) curves show the same distribution for the SARCS lens population with arbitrary normalization (More et al. 2012).

We produce catalogs with lens and source properties for each of the three types of lenses. These catalogs are available XXX. The catalogs typically have lens position, redshift, magnitudes, Einstein radius, ellipticity (whenever available) and shear (for galaxy-scale lenses only). For the background sources, we provide the offset from the lens center, redshift, magnitudes, total magnification, number of lensed images. Additionally, ellipticity and effective radius when the background sources are galaxies.

### 3.3 Limitations of the simulated sample

The simulated sample is not perfect because our understanding of various phenomena in the Universe is not complete and because of the uncertainties in the parameters of our model. Here, we describe some of the cases or aspects in which the simulations are known to have failed or seem unrealistic.

The parameters required by various scaling relations and the models primarily depend on the photometry of the galaxies, groups and quasars detected in the survey. For galaxy-scale lenses, the lensing galaxies at higher redshifts or which are fainter have poor photometric measurements. This causes relatively larger uncertainties in its luminosity and velocity dispersion and leads to simulated lenses which look implausible. For example, due to a larger uncertainty in the velocity dispersion of the lensing galaxy, the lensed images may have larger image separation than what is expected given the visual priors from the galaxy.

At group-scales, the photometric and redshift estimates are used when defining the group membership. Therefore, errors in redshift estimates generate galaxy groups with BGG or member galaxies with dissimilar properties. In some cases, low redshift spiral galaxies are incorrectly assigned high redshift. Spiral galaxies are typically less massive and low redshift spiral galaxies are unlikely to act as gravitational lenses. Hence, the resulting simulated lenses are not convincing.

We use single Sersic component to describe the light profiles of background galaxies. This is clearly not the most accurate description for galaxies, especially, star-forming galaxies which form a significant fraction of the lensed galaxy population. Star-forming galaxies have complex structures such as star forming knots, spiral arms, bars and disks.

## 4 TRAINING SAMPLE: DUDS AND FALSE POSITIVES

A good training sample consists of a representative set of objects that one wants to find and another set of objects which appear to be from the former set but are of different origin in reality and which one can learn to discard efficiently. Indeed, we wanted to have a good training sample for the Space Warps users so that they can correctly identify the true lens candidates. Hence, in addition to the simulated lenses, we added a sample of duds and false positives to the training sample. Duds are images which have been visually inspected by experts and confirmed to contain no lenses. False positives are systems which look like lenses but are not, for example, spiral galaxies, starforming galaxies, chance alignments of features arranged in a lensing configuration and stars.

We selected a sample of 450 duds for the Stage I classification in Space Warps and a sample of 500 false positives for the Stage II inspection. The sample of false positives was selected from the candidates which passed the Stage I of Space Warps. We note that this is the first time, we have a systematically compiled sample of visually inspected false positives by the Space Warps users and categorized by the science team. Such a sample is tremendously helpful for training and understanding performances of various lens finding algorithms (Chan et al. 2014). **TBA data products; make the duds and FP sample available**

## 5 RESULTS

### 5.1 Space Warps Lens Sample

The Space Warps works as a single unified neural network which uses the method of visual inspection to find gravitational lenses. The citizens are shown images at two stages. At stage I, citizens focus on rapid inspection and selection of lens candiates ranging from possible lenses to almost certain lenses. At stage II, citizens carefully inspect the candidates from stage I and select promising lens candidates only. The science team consisting of lens experts then categorize and grade the lens candidates further purifying the sample of lens candidates. In Table 2, we list the total number of detections of the known lens candidates, known confirmed lenses and the new lens candidates at both stages I and II. The known sample corresponds to the combined Ring Finder and Arc Finder samples. We also show their fractions with respect to the total number of lens candidates found at these stages. We note that all the confirmed lenses found at stage I are also recovered at stage II whereas a small fraction of the known lens candidates are rejected at stage II. Also, the new lens candidates increases the known lens candidates sample by over 50%.

Below, we describe the steps taken after stage II for selecting the final sample of lens candidates.

#### 5.1.1 *Selection of the Space Warps lens candidates*

The images inspected in Space Warps are assigned probabilities (P) through the Space Warps Analysis Pipeline (SWAP), built in the Space Warps system (see Paper I). In an ideal situation, at the end of stage II, all images containing lenses would have high P values and those without lenses will have low P values. However, practically, a fraction of the real lenses will be assigned low P value decreasing the completeness and a fraction of non-lenses will be assigned high P value decreasing the purity. Our goal is to find a P value which will result in acceptable levels of completeness and purity of the final sample of lens candidates.

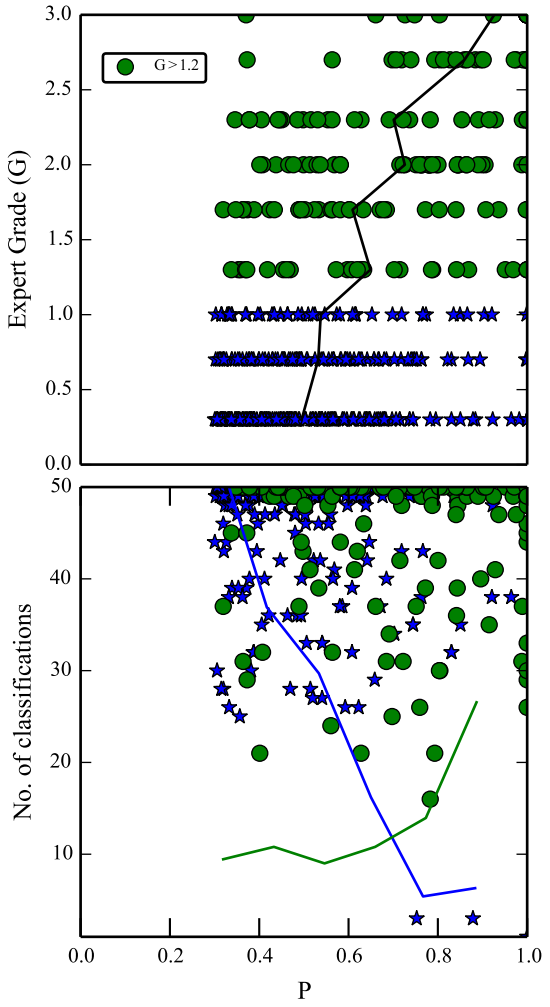


**Figure 4.** Comparison of the P(lens) with the expert grades and number of classification for each subject.

As this is the first Space Warps lens search, we explore a large range in the P value to understand the balance between the real lens candidates and false positives. In Figure 4, we plot the distribution of false positives and real lens candidates categorized by the lens experts as a function of their P value. As expected, the fraction of real lens candidates is higher for higher P values and it decreases for lower P values. We note that from P∼0.7 onwards to lower P values, the fraction of false positives starts to exceed the fraction of real lens candidates. This could be a good threshold to choose to maximize the purity of the final sample. However, we choose P>0.3 as our threshold to increase the completeness of our sample. We achieve further purity by including the grades of the lens experts.

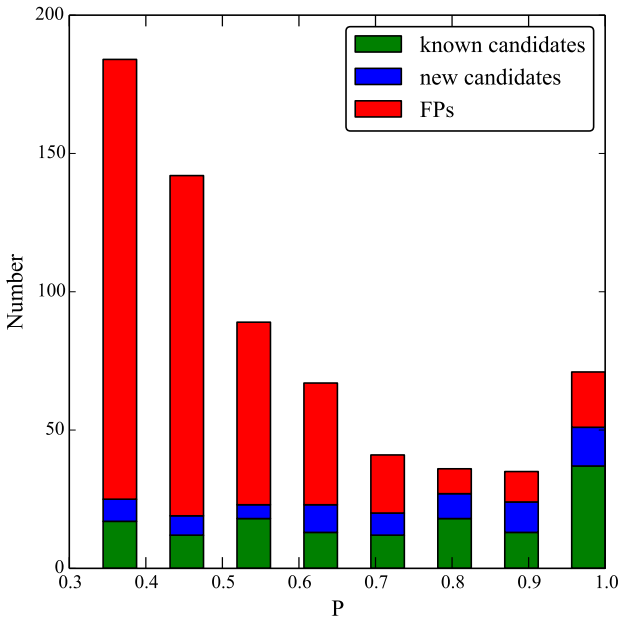


**Figure 5.** Total number of detections of the known candidates, new candidates and the FPs shown relatively for binned values of P.

**Table 2.** Statistics of detections in Space Warps

| | Stage I | | Stage II | | | |
|---|---|---|---|---|---|---|
| | KC | KL | KC | KL | NC | AC |
| Number | 128 | 34 | 107 | 34 | 61 | 168 |
| % | 29 | 58 | 25 | 58 | 12 | 34 |
| $P_{thresh}$ | 0.95 | 0.95 | 0.3 | 0.3 | 0.3 | 0.3 |

KC– Known lens candidates
KL– Known confirmed lenses
NC– New lens candidates
AC– All (known and new) lens candidates
$P_{thresh}$ – systems with P above this threshold are selected
Note about %: For KC and KL, fractions are with respect to the known population whereas for NC and AC, fractions are with respect to the total population of lens candidates.

#### *5.1.2 New lens candidates from* Space Warps

All images with P>0.3, at the end of stage II, are inspected by three lens experts (AM, AV, PJM) and are assigned integral grades from 0,1,2 or 3 which imply that the candidate is almost certainly not a lens, possibly a lens, probably a lens and almost certainly a lens, respectively. This process led to a final sample of 61 new lens candidates with averaged grade $\geqslant$1.3 (see Table 3) and are shown in Figure 6. For this final sample, we give a Space Warps ID and Name of the lens system, Ra, Dec, photometric redshift ($z_{phot}$), $i$ band magnitude of the lensing galaxy, averaged grade from the lens experts, zoo ID (identifier used in TALK[7], the discussion forum for Space Warps), P value at stage II and a visual categorization of type of lensed images and the lensing galaxy in the Comments column in Table 3. Whenever available the lens properties are taken from the CFHTLS photometric catalog (Coupon et al. 2009) otherwise the reported lens galaxy positions are measured visually. The visual categorization of the lens type is only suggestive and the explanation of the notations in the Comments column is given at the bottom of the table.

As the first lens search was a blind search with no preselection of candidates using any algorithm, we expected to find various types of lenses and this is indeed what we find. The final sample consists of both galaxy and groups-scale lens candidates. There are detections of elongated arcs and point-like quasar lensed images. Most of them are brighter in bluer $g$ band but some candidates brighter in the redder $i$ band are also found.

**CHECK FOR STAGE 1 – COMPLETENESS OF SIMS AND KNOWN LENSES and P value comparison, what about the duplicate lenses near the borders - stats on those? check the detection plot of arc mag / Reinst and find out why some of the bins have unexpected results**

### 5.2 Measurements of lens and arc properties

In the subsequent sections, we make comparison of various properties of the lens candidates. Here, we describe how we measured those properties, namely, the lens redshift, the Einstein radii and the total flux of the arcs.

We use the publicly available redshifts for the lens galaxy from the CFHTLS photometric catalogs (Coupon et al. 2009). The definition of the Einstein radius is different in different cases. For the galaxy-scale lenses in the simulated sample, we use the value of the input lens model parameter for the $R_{\rm E}$. For groups-scale lenses, since the lens model is multi-component, we need to determine the $R_{\rm E}$ from the image positions. We use half of the averaged image separations of the lensed image counterparts with minimum and maximum image separations. For the RingFinder sample, the arcs are detected in the scaled difference image between $g$ and $i$ bands where the lensing galaxy is subtracted (Gavazzi et al. 2014, for details, see). We use the peak position of the lensed images measured by running sextractor on this difference image and identified visually. We calculate the image separation from the lens center as an estimate of the $R_{\rm E}$. For the ArcFinder (SARCS) sample, we use the same definition as above except that the peak position is identified either by the ArcFinder or visually. For the Space Warps lens sample, the same definition is used where the peak positions are identified either with ArcFinder or sextractor.

The total flux of the arc is measured in the $g$ band. For the simulated sample, we multiply the magnification of the second brightest image with the source magnitude. For the RingFinder sample, we use the flux of the lensed images measured by sextractor from the scaled difference image, that is, $g - \alpha i$ and convert it to the $g$ band flux using mean colors of the foreground and background population. For the ArcFinder and the Space Warps sample, we integrate the flux in the image pixels identified by ArcFinder or sextractor.

[7] http://talk.spacewarps.org/

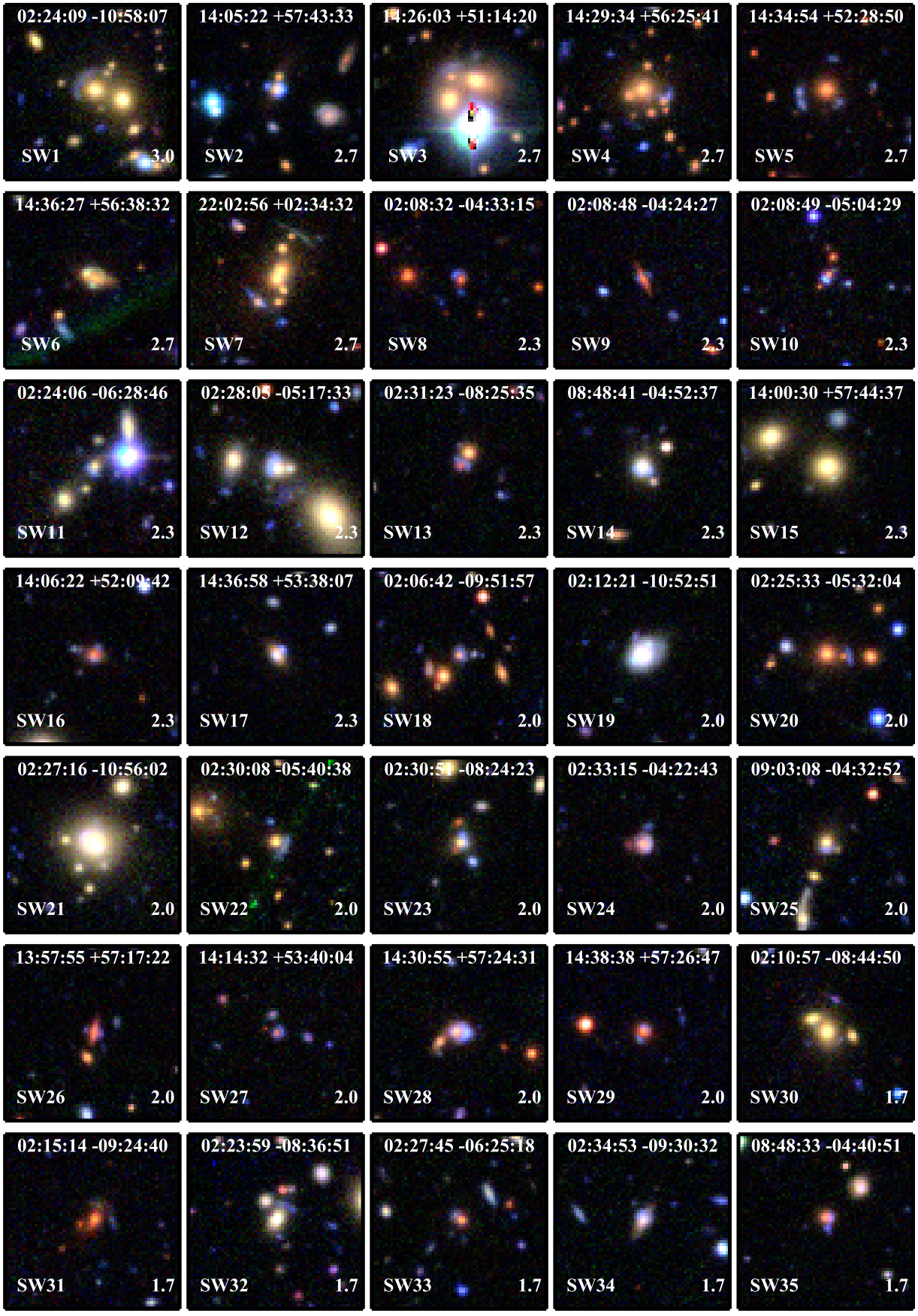
02:24:09 -10:58:07
SW1 3.0
14:05:22 +57:43:33
SW2 2.7
14:26:03 +51:14:20
SW3 2.7
14:29:34 +56:25:41
SW4 2.7
14:34:54 +52:28:50
SW5 2.7
14:36:27 +56:38:32
SW6 2.7
22:02:56 +02:34:32
SW7 2.7
02:08:32 -04:33:15
SW8 2.3
02:08:48 -04:24:27
SW9 2.3
02:08:49 -05:04:29
SW10 2.3
02:24:06 -06:28:46
SW11 2.3
02:28:05 -05:17:33
SW12 2.3
02:31:23 -08:25:35
SW13 2.3
08:48:41 -04:52:37
SW14 2.3
14:00:30 +57:44:37
SW15 2.3
14:06:22 +52:09:42
SW16 2.3
14:36:58 +53:38:07
SW17 2.3
02:06:42 -09:51:57
SW18 2.0
02:12:21 -10:52:51
SW19 2.0
02:25:33 -05:32:04
SW20 2.0
02:27:16 -10:56:02
SW21 2.0
02:30:08 -05:40:38
SW22 2.0
02:30:51 -08:24:23
SW23 2.0
02:33:15 -04:22:43
SW24 2.0
09:03:08 -04:32:52
SW25 2.0
13:57:55 +57:17:22
SW26 2.0
14:14:32 +53:40:04
SW27 2.0
14:30:55 +57:24:31
SW28 2.0
14:38:38 +57:26:47
SW29 2.0
02:10:57 -08:44:50
SW30 1.7
02:15:14 -09:24:40
SW31 1.7
02:23:59 -08:36:51
SW32 1.7
02:27:45 -06:25:18
SW33 1.7
02:34:53 -09:30:32
SW34 1.7
08:48:33 -04:40:51
SW35 1.7

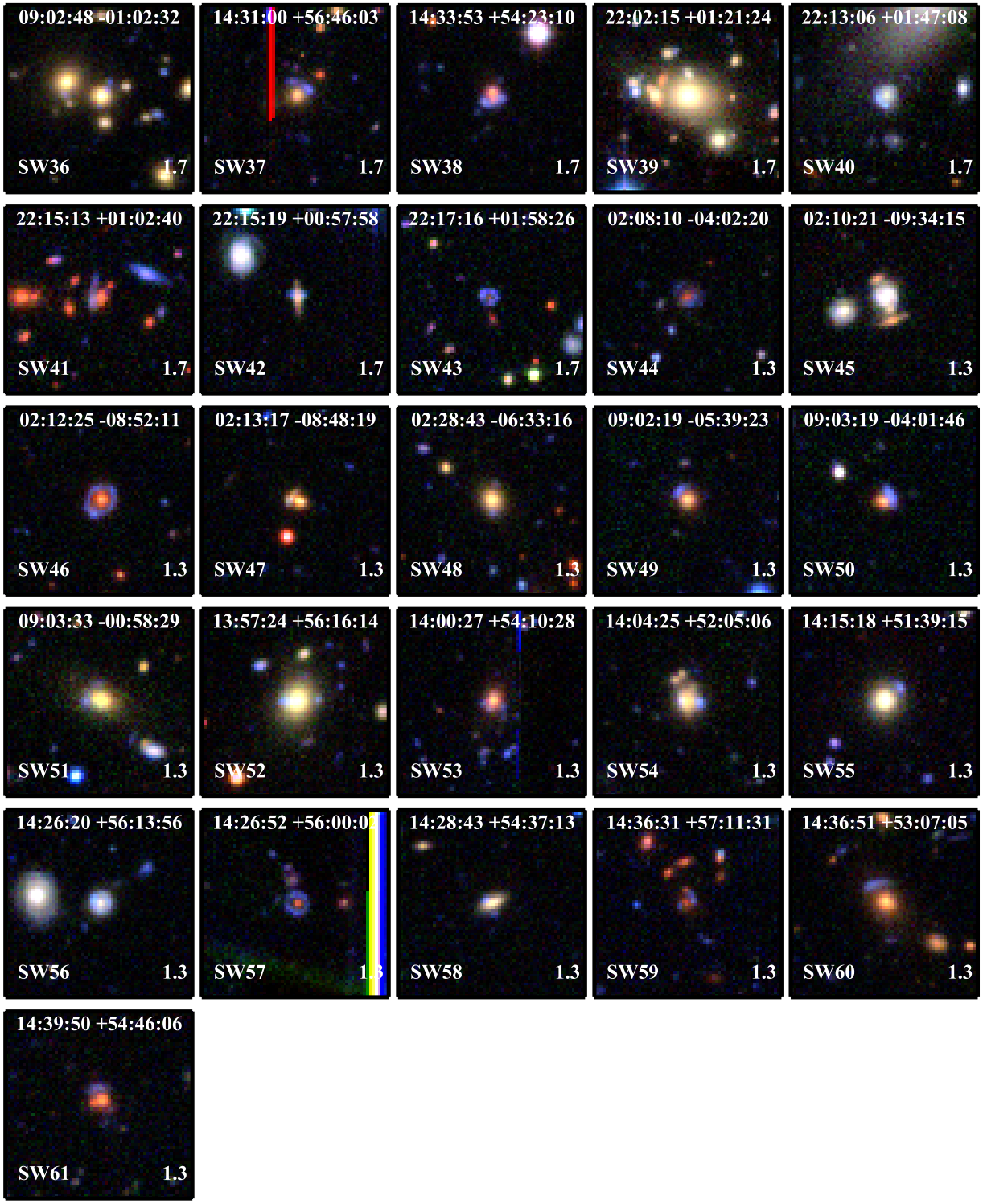


**Figure 6.** Sample of lens candidates with G>=1.3.

### 5.3 Recovery of known CFHTLS lenses with Space Warps

We determine what fraction of the known sample of lenses are recovered by Space Warps. In Table 2, we show that $\sim$ 25%-30% of the known candidates and $\sim$ 60% of the known confirmed lenses are found at stages I and II in Space Warps. The left and the middle panels of Figure 7 show the fraction of detections as a function of arc magnitude and the Einstein radius of the lens systems.

As expected, we find that systems with brighter images and/or with larger Einstein radii are detected more often in Space Warps.

We find that most of the confirmed lenses and candidates that are missed by Space Warps are systems with fainter arcs and smaller Einstein radii and they come from the RingFinder sample. The main reason why RingFinder found such candidates is because their team used lensing galaxy-subtracted images to detect the presence of the lensed images both during the automated object-finding phase and during the visual inspection and classification of their candidates. This approach naturally improves the detection efficiency at smaller Einstein radii and for fainter systems. The Space Warps volunteers were not shown any galaxy-subtracted images. However, in light of the improved detection efficiency, this might be a better strategy to adopt for future lens searches at galaxy-scales with Space Warps. In the Discussion Section 6.2, we further explore and discuss why the confirmed lenses may have been missed in Space Warps.

### 5.4 Image separation distribution

The distribution of image separations (i.e. twice the Einstein radius) can be used to probe the average density profile of the lens population (Oguri 2006; More et al. 2012). However, the lens sample found by the Arc Finder may have incompleteness as a function of the image separation. Thus, the lack of understanding of the selection function of the lens sample may affect the constraints on the density profile. A blind lens search done by visual inspection alone e.g. by Space Warps may find lenses missed by the Arc Finder search and thereby, improve completeness. Furthermore, the completeness of the lens sample found by Space Warps is characterised with the help of the simulated sample. For example, in the right most panel of Figure 7, we plot the completeness of the simulated sample found at stage I of Space Warps as a function of the arc magnitude and Einstein radius. We find that the sample is more than 80% complete between image separations 2"-10".

In Figure 10, we plot theoretical curves for the image separationd distribution corresponding to three density profiles, namely, isothermal sphere (IS), NFW (Navarro et al. 1997) and Total profile which has NFW and Hernquist profiles combined with an adiabatically contracting model for dark matter component (Gnedin et al. 2004) taken from More et al. (2012).

## 6 DISCUSSION

Finding gravitational lenses is a difficult and complex task. No one method is perfect. Each method has some advantages over the other. It may be the case that a single method may not be the best means for optimising completeness and purity. Visual inspection will likely be required for pruning candidates at some stage of lens candidate selection even in the future. Therefore, we would like to understand how best we should combine the strengths of robots and humans to optimize the lens finding method.

In this section, we attempt to understand and compare the lens (candidates) that are found by the lens finding robots and missed by humans and vice versa.

### 6.1 Why Space Warps candidates were missed by lens finding robots?

We rerun the RingFinder and ArcFinder on images centered on the new Space Warps candidates to trace and understand at what stage the algorithm failed to detect them.

First, we rerun RingFinder on the new Space Warps sample. At the beginning, a galaxy catalog is generated based on magnitude, redshift and SED type (Gavazzi et al. 2014, see) to select galaxies which are most likely to act as lenses. We find that about 40% of the new Space Warps candidates fail to meet this initial selection criteria e.g. SW1, SW13, SW19, SW22, SW27 and SW30. All of the lensing galaxies are bright enough to satisfy the $i < 22$ criterion. However, some of them have a bright companion galaxy, some of them do not look like E/S0 type galaxies and some are edge on galaxies. **there are a few which look regular galaxies so which criteria are they failing??**

In the following steps, the flux from the galaxy is subtracted from the scaled difference image to enhance the visibility of the faint blue lensed features. An object finder is run on this image to quantify the lensed image properties. About 50% of the Space Warps candidates could not be detected by the object finder because properties such as the image area, axis ratio, magnitude/color and alignment with respect to the lensing galaxy are not satisfied. Some of the candidates missed at this stage are e.g. SW4, SW5, SW6, SW26, SW36, SW39 and SW47.

Next, we rerun the ArcFinder on the same Space Warps sample of new candidates. The ArcFinder is directly run on images to look for elongated arc like objects and does not require a list of targets to begin with. Objects are identified by placing thresholds on the noise level in the images. Thus, ArcFinder detections are sensitive to changes in the noise levels.

Originally, the ArcFinder was run on a large image with an area of $\sim 19350 \times 19350$ pixels$^2$. For the rerun, we work with much smaller images because this is faster but this alters the measured noise and hence, affects the number and type of arc detections. We find that about 30% of the new candidates are detected without changing any of the thresholds in the code because of the change in the noise level. **does this make sense?**

The ArcFinder code calculates second order brightness moments around every pixel to decide if the distribution of flux is elongated in some direction in order to detect elongated arc-like objects. An elongation estimator is assigned to every pixel. All pixels with a value of the estimator above a certain threshold are connected to form the arc feature. This is building of the arc candidate. Subsequently, arc properties such as the area, mean flux, length and curvature are determined. We relax the threshold at the building stage and also relax thresholds mainly on the area of the arc which leads to detection of about 75% of the new Space Warps candidates. We find that relaxing thresholds on other arc properties do not improve the detection rate significantly and thus are left unchanged.

Typically, the candidates are missed from the ArcFinder sample if a) they are brighter in the redder band

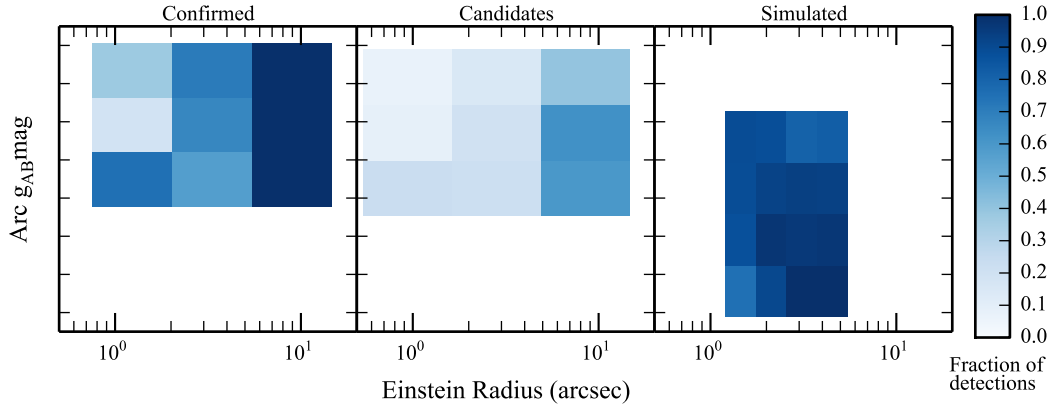


**Figure 7.** Fraction of lens candidates detected by Space Warps as a function of the arc magnitude ($g$ band) and the Einstein radius for three lens samples, namely, simulated lenses, known confirmed lenses and the lens candidates sample.

rather than the bluer $g$ band used for arc detection because then the arc feature will be at the noise level and will fail detection b) the flux of the arc and the galaxy are blended in the $g$ band such that the ArcFinder mistakenly connects part of the galaxy to the pixels belonging to the arc candidate which then results in a candidate with no morphological characteristics of an arc or c) if the candidate is not elongated which means most of the lensed quasars with circular looking lensed images will be missed.

Relaxing the thresholds obviously increases the total number of candidate detections which includes a large sample of false positives. For example, the number of arc candidate detections increase by a factor of ∼2 when we relaxed the thresholds in the reruns described above whereas the number of false positives increase by a factor of ∼5. Thus, it is not recommended to relax these thresholds alone. A better alternative is to relax the thresholds to increase the completeness and cross-correlate the arc candidate positions with a galaxy catalog to discard those candidates which are not close to a putative lensing galaxy within typical radius in order to reduce the false positives.

**TBD: comment on any lensed quasars, on any exotic lenses; of course, there must be lenses which cannot be detected currently by either robots/humans check if some candidates were detected because they were hidden underneath the sims ie. from the D11;**

## 6.2 False negatives: known lenses missed by Space Warps

Like any lens finding method, the Space Warps system can fail to detect certain kinds of lenses. Here, we explore and discuss why some of the known lenses may have been missed.

We find that about 40% of the known confirmed sample of lenses are missed (see Table 2). While this seems like a fraction, we note that many of the missed lenses are from the RingFinder sample with small Einstein radii and faint lensed images (see Figure 7). Among the confirmed lenses from the RingFinder, about 50% are missed. Out of the missed sample of 18 lenses, about half of them are visually difficult to detect and the other half appear to have faint blue smudges around galaxies which should have been easier to identify. Similarly, if we consider the ArcFinder lens sample, ∼23% are missed by Space Warps. This is a relatively small sample of ∼ 5 systems and visual inspection suggests that, by and large, either the lensed features are faint or they have odd properties which makes them difficult to identify correctly. (**show some example images XXX**). For further tests, we combine the RingFinder and ArcFinder sample.

For a lens finding method which uses collective skill, experience and knowledge of a group of citizens, it may be difficult to find a single factor with certainty which causes a lens candidate to be missed. We attempt to understand whether there is indeed a single dominant factor that is resulting in the loss of these lenses or the lenses are being missed due to a combination of multiple reasons. Below, we consider some of the factors that could affect the efficiency of finding lenses.

First, we check if the Nclass is different for the detected and the missed sample. Surprisingly, most of the lenses in the known sample have few classifications (Nclass¡10) which includes both the detected and missed lenses. Many of the remaining have between 10 to 20 classifications. And, only a few subjects have Nclass¿20 which continue to remain for long in the database because these candidates may have been difficult to identify.

### *6.2.1 Blind lens search*

Efficiency of a visual search can vary in different sections of an image. Our eyes tend to focus usually at the center of an image and lens candidates close to the borders could go undetected. Therefore, it is essential to test and understand if Space Warps tends to miss certain lenses because they happen to be close to the borders of the image cutouts.

From the SWAP, the image cutouts inspected by the Space Warps volunteers receive a status of detected (if $P > P_{accthresh}$), rejected (if $P < P_{rejthresh}$) and undecided (if $P_{rejthresh} < P < P_{accthresh}$). In Figure 11, we compare the positions of simulated lenses which are detected (red), undecided (green) and rejected (blue). We also make the same comparison for the known lens candidates in the right panel.

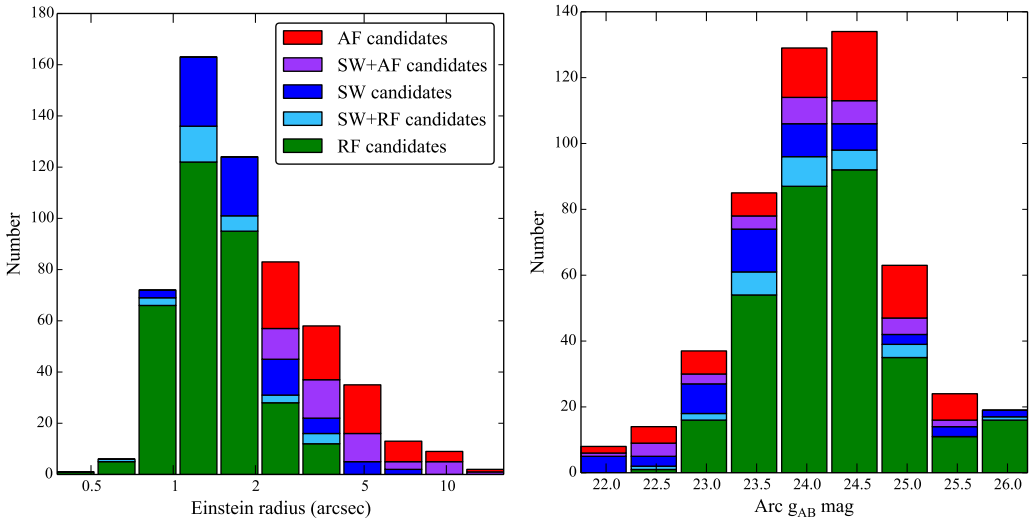


**Figure 9.** Candidate detections by the RINGFINDER, SPACE WARPS and the ARCFINDER as a function of the Einstein radius and $g$ band magnitude of the lensed images. (XXXX check how different are the estimates from the different measurement techniques for a given lens candidates.)

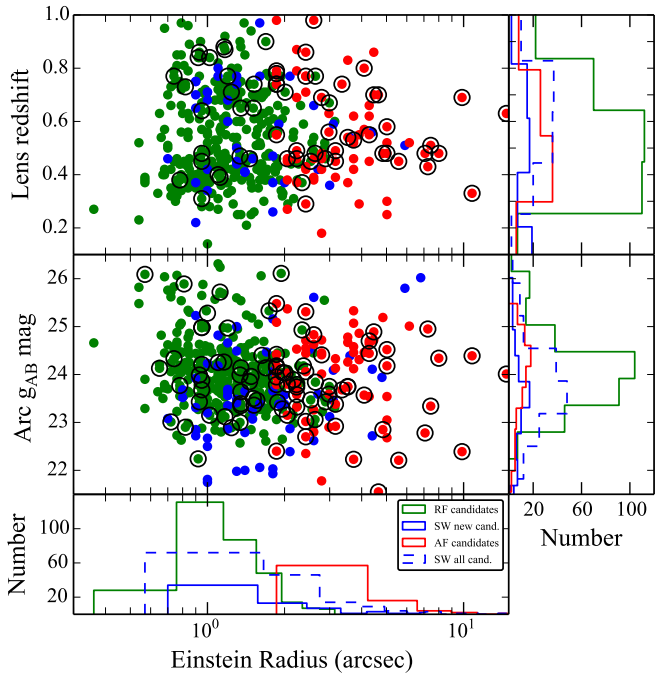


**Figure 8.** Comparison of the lens redshift and of the arc magnitude with the Einstein radius for all of the three lens samples, namely, from the RINGFINDER (green dots), SPACE WARPS (all candidates black circles and new candidates only in blue dots) and ARCFINDER (red dots).

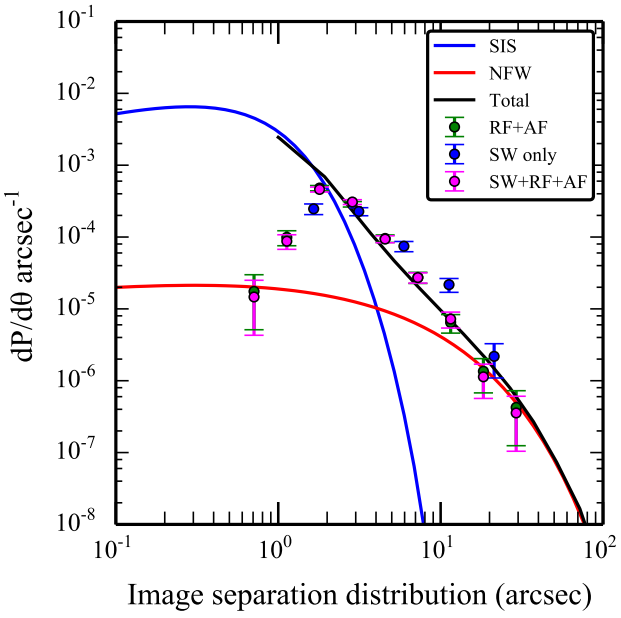


**Figure 10.** Image separation distribution. Comparing theoretical predictions (solid curves) with the CFHTLS known lens samples (REF , green points) and the same CFHTLS sample after combining with the incremental lens sample from SPACE WARPS (magenta points). The SPACE WARPS only sample including new and known lens candidates are shown with blue points.

We note that for some cases randomly selected subsamples are shown for the ease of visual comparison. For example, the absolute number of simulated lenses detected is too high compared to the rejected sample. We do not find any strong visual correlation in the rate of detections as a function of the position for both the simulated and the known lens sample. Thus, the completeness of the lens sample does not seem to be significantly affected by whether a lens is located close to the border or well within the center.

### 6.2.2 *Volunteer profile*

Here, we investigate if the skill or experience of volunteers is systematically different between the sample of detected and missed lenses.

We check how the posterior probability P (see XXXX Paper I) of an image or a subject to contain a lens changes as the image receives more classifications from multiple users. In Figure 12, we show the trajectory plots of a few examples of detected lenses (top left panels) and missed lenses (bottom left panels) by Space Warps at stage I. The number of classifications (Nclass) for a subject increase from top to bottom. Also, every subject is assigned a prior probability P0=2.e-4 (grey dashed line) and starts at the middle of the trajectory plot. The P value of a subject is updated with every classification from the volunteer. If a volunteer identifies a lens candidate, the trajectory moves to the right otherwise moves to the left. A subject is accepted if it crosses the blue-dashed line marking the ($P_{accthresh} = 0.95$) on the right and is rejected, if it crosses the red-dashed line marking the $P_{rejthresh} = 1.e - 7$ on the left.

By how much the P value will change depends on how well the volunteers are performing on the training sample. Thus, more skilled volunteers will change the P by a large factor compared to the less skilled volunteers. This is evident in the trajectory plots as large and small distances in between consequent points.

## 7 SUMMARY AND CONCLUSIONS

In this paper, we describe the framework and procedure used to generate simulated lens sample for the blind lens search in the CFHTLS survey in collaboration with Space Warps. The aim of this lens search is to find lenses that have been missed by lens finding algorithms. The simulated lens sample is used for training the citizen scientists, calibrating their performance and rejecting unlikely lenses from the sample based on the classifications of citizen scientists. As a result, the simulated lenses need to consist of realistic looking lenses.

We use the photometric and redshift catalogues for the foreground galaxies and additionally, color catalogues for background galaxies and quasars. We use scaling relations to relate light properties to properties such as mass and size to generate lens models. We further account for the instrumental effects such as seeing and noise before creating the final lensed images of model background sources. We add the lensed images on top of the real galaxies and groups in the CFHTLS data in all filters.

We draw the following conclusions:

- Crowd-sourced gravitational lens detection works, as shown in by comparing with real lenses in CFHTLS: Real (robotically-detected and expert-confirmed) lenses are recovered/missed at similar/comparable/different rates C% and P% - this is a partial test of supervised vs unsupervised learning
- We found a sample of new gravitational lens candidates. An expert-graded sample of 74 with 44 promising and 30 low probability candiates.

The SW lenses are different from the robotically (RingFinder and ArcFinder) detected lenses, in the following ways. XXXXX

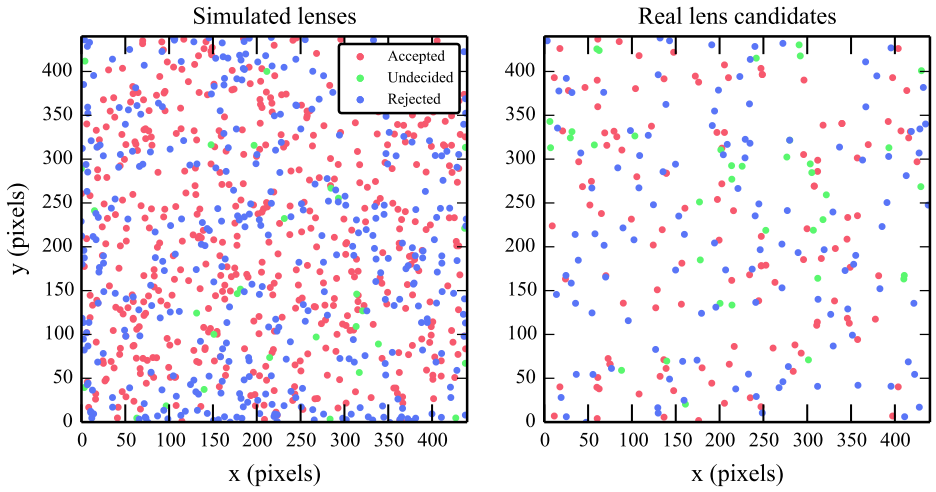


**Figure 11.** Completeness as a function of position of lens systems. Simulated lenses (left) and real lens candidates (right) are shown. Irrespective of the status of the lenses, that is, detected, undecided or rejected, there is no strong dependency on where the lenses are located both for the simulated and the real sample of lens candidates.

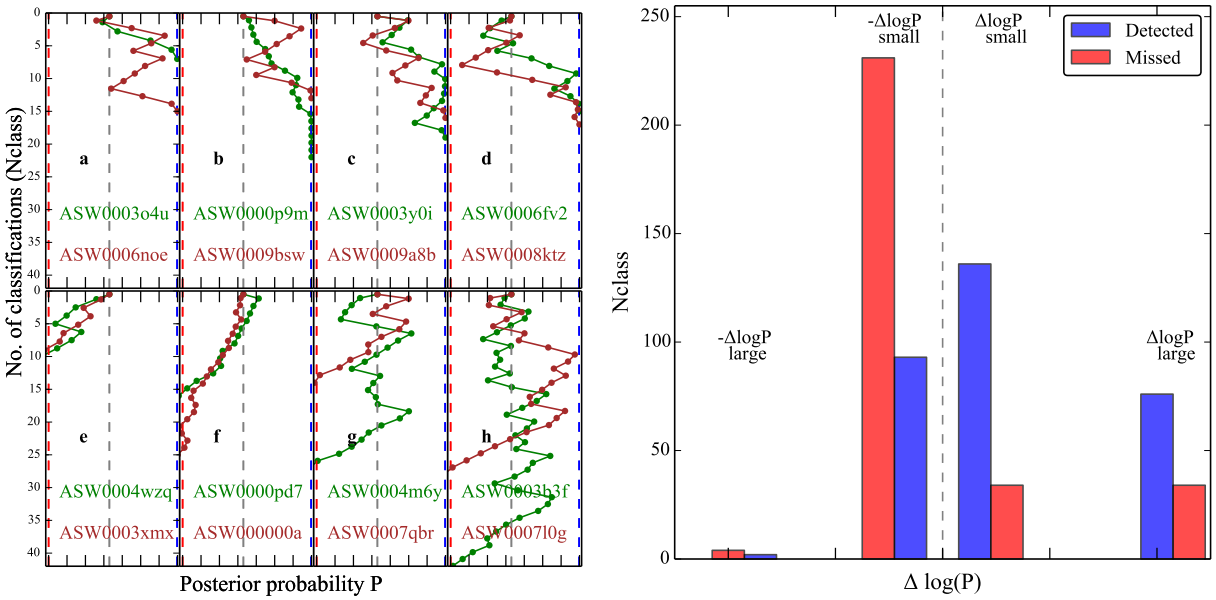


**Figure 12.** Example cases of trajectories of known lenses on the left and histogram of the known lenses. The trajectories on the left are lenses that are detected by Space Warps are at the top and lenses that are missed are at the bottom.

Table 3: Sample of the Space Warps new lens candidates.

| SW ID | Name | RA (deg) | Dec (deg) | $z_{\rm phot}$ | $m_i$ (mag) | $R_{\rm A}$ (") | G | ZooID | P | Comments |
|---|---|---|---|---|---|---|---|---|---|---|
| SW1 | CFHTLS J022409-105807 | 36.0398 | -10.9688 | 0.0 | 0.0 | 4.8 | 3.0 | ASW0004dv8 | 1.0 | A,G |
| SW2 | CFHTLS J140522+574333 | 211.3426 | 57.7259 | 0.7 | 19.7 | 1.0 | 2.7 | ASW000619d | 0.7 | A,R |
| SW3 | CFHTLS J142603+511420 | 216.5149 | 51.2390 | 0.0 | 0.0 | 4.4 | 2.7 | ASW0006mea | 0.7 | A,G |
| SW4 | CFHTLS J142934+562541 | 217.3926 | 56.4281 | 0.5 | 19.0 | 5.9 | 2.7 | ASW0009cjs | 0.8 | A,G |
| SW5 | CFHTLS J143454+522850 | 218.7270 | 52.4808 | 0.6 | 19.4 | 4.4 | 2.7 | ASW0007k4r | 0.4 | Q,G/R |
| SW6 | CFHTLS J143627+563832 | 219.1164 | 56.6425 | 0.5 | 19.4 | 1.5 | 2.7 | ASW0008swn | 0.9 | A,D |
| SW7 | CFHTLS J220256+023432 | 330.7369 | 2.5758 | 0.0 | 0.0 | 6.8 | 2.7 | ASW0007e08 | 0.8 | A,G/C |
| SW8 | CFHTLS J020832-043315 | 32.1340 | -4.5543 | 1.0 | 21.0 | 1.6 | 2.3 | ASW0002asp | 1.0 | A,R |
| SW9 | CFHTLS J020848-042427 | 32.2011 | -4.4075 | 0.8 | 20.5 | 1.1 | 2.3 | ASW0002bmc | 0.9 | D,D |
| SW10 | CFHTLS J020849-050429 | 32.2078 | -5.0749 | 0.8 | 20.6 | 0.9 | 2.3 | ASW0002qtn | 1.0 | A,R |

| SW ID | Name | RA (deg) | Dec (deg) | $z_{\rm phot}$ | $m_i$ (mag) | $R_{\rm A}$ (") | G | ZooID | P | Comments |
|---|---|---|---|---|---|---|---|---|---|---|
| SW11 | CFHTLS J022406-062846 | 36.0256 | -6.4796 | 0.4 | 19.6 | 0.9 | 2.3 | ASW0003wsu | 0.7 | A,E |
| SW12 | CFHTLS J022805-051733 | 37.0236 | -5.2927 | 0.4 | 18.8 | 1.4 | 2.3 | ASW0009ans | 1.0 | Q,E |
| SW13 | CFHTLS J023123-082535 | 37.8468 | -8.4266 | 0.0 | 0.0 | 1.2 | 2.3 | ASW0004xjk | 0.3 | A,R |
| SW14 | CFHTLS J084841-045237 | 132.1708 | -4.8772 | 0.3 | 19.0 | 1.0 | 2.3 | ASW0004nan | 1.0 | A,E |
| SW15 | CFHTLS J140030+574437 | 210.1260 | 57.7437 | 0.4 | 18.2 | 2.0 | 2.3 | ASW0009bp2 | 0.6 | A,E |
| SW16 | CFHTLS J140622+520942 | 211.5958 | 52.1617 | 0.7 | 20.3 | 1.2 | 2.3 | ASW0005rnb | 0.7 | A,R |
| SW17 | CFHTLS J143658+533807 | 219.2425 | 53.6355 | 0.7 | 19.6 | 0.9 | 2.3 | ASW0007hu2 | 0.6 | D,D |
| SW18 | CFHTLS J020642-095157 | 31.6750 | -9.8658 | 0.2 | 20.8 | 0.9 | 2.0 | ASW0001ld7 | 0.8 | A,R |
| SW19 | CFHTLS J021221-105251 | 33.0881 | -10.8811 | 0.3 | 17.9 | 1.8 | 2.0 | ASW0002dx7 | 0.8 | D,E/S |
| SW20 | CFHTLS J022533-053204 | 36.3888 | -5.5346 | 0.5 | 19.4 | 3.6 | 2.0 | ASW0004m3x | 0.4 | A,R/G |
| SW21 | CFHTLS J022716-105602 | 36.8186 | -10.9341 | 0.4 | 17.2 | 1.8 | 2.0 | ASW0009ab8 | 0.7 | A,E/G |
| SW22 | CFHTLS J023008-054038 | 37.5359 | -5.6774 | 0.6 | 19.7 | 1.9 | 2.0 | ASW0003r61 | 0.5 | A,E |
| SW23 | CFHTLS J023051-082423 | 37.7141 | -8.4064 | 0.0 | 0.0 | 0.8 | 2.0 | ASW000412m | 0.4 | A,E |
| SW24 | CFHTLS J023315-042243 | 38.3133 | -4.3789 | 0.7 | 19.7 | 1.0 | 2.0 | ASW00050sk | 0.8 | A,R |
| SW25 | CFHTLS J090308-043252 | 135.7844 | -4.5479 | 0.0 | 0.0 | 1.2 | 2.0 | ASW00007mq | 0.6 | A,E |
| SW26 | CFHTLS J135755+571722 | 209.4827 | 57.2897 | 0.8 | 20.2 | 1.3 | 2.0 | ASW0005ma2 | 0.8 | D,D |
| SW27 | CFHTLS J141432+534004 | 213.6372 | 53.6679 | 0.7 | 21.4 | 0.9 | 2.0 | ASW0006jh5 | 0.8 | A,R |
| SW28 | CFHTLS J143055+572431 | 217.7333 | 57.4088 | 0.7 | 19.3 | 1.0 | 2.0 | ASW0007wfj | 0.9 | A,R |
| SW29 | CFHTLS J143838+572647 | 219.6589 | 57.4464 | 0.8 | 20.2 | 1.1 | 2.0 | ASW0008qsm | 0.9 | A,R |
| SW30 | CFHTLS J021057-084450 | 32.7414 | -8.7474 | 0.0 | 0.0 | 2.5 | 1.7 | ASW0002p8y | 0.4 | A,G |
| SW31 | CFHTLS J021514-092440 | 33.8109 | -9.4111 | 0.7 | 19.9 | 2.6 | 1.7 | ASW00021r0 | 0.4 | A,R/G |
| SW32 | CFHTLS J022359-083651 | 35.9995 | -8.6143 | 0.0 | 0.0 | 3.1 | 1.7 | ASW0004iye | 0.4 | A,E |
| SW33 | CFHTLS J022745-062518 | 36.9387 | -6.4218 | 0.6 | 20.5 | 1.2 | 1.7 | ASW0003s0m | 0.5 | A,R |
| SW34 | CFHTLS J023453-093032 | 38.7232 | -9.5089 | 0.5 | 19.8 | 0.7 | 1.7 | ASW00051ld | 0.3 | A,D |
| SW35 | CFHTLS J084833-044051 | 132.1385 | -4.6809 | 0.8 | 20.2 | 0.9 | 1.7 | ASW0004wgd | 0.7 | A,R |
| SW36 | CFHTLS J090248-010232 | 135.7020 | -1.0424 | 0.4 | 19.1 | 1.4 | 1.7 | ASW000096t | 0.6 | D,E |
| SW37 | CFHTLS J143100+564603 | 217.7511 | 56.7675 | 0.0 | 0.0 | 1.8 | 1.7 | ASW00086xq | 0.8 | A,E |
| SW38 | CFHTLS J143353+542310 | 218.4736 | 54.3862 | 0.8 | 19.8 | 1.6 | 1.7 | ASW0009cox | 0.6 | A,R/G |
| SW39 | CFHTLS J220215+012124 | 330.5635 | 1.3567 | 0.3 | 17.4 | 4.6 | 1.7 | ASW0005qiz | 0.5 | rA,G |
| SW40 | CFHTLS J221306+014708 | 333.2758 | 1.7856 | 0.0 | 17.1 | 1.4 | 1.7 | ASW0008wmr | 0.9 | A,S |
| SW41 | CFHTLS J221513+010240 | 333.8056 | 1.0446 | 0.0 | 0.0 | 0.8 | 1.7 | ASW0008dxh | 0.3 | A,R/G |
| SW42 | CFHTLS J221519+005758 | 333.8321 | 0.9661 | 0.4 | 20.2 | 1.0 | 1.7 | ASW0008xbu | 0.8 | A,D |
| SW43 | CFHTLS J221716+015826 | 334.3189 | 1.9739 | 0.1 | 21.6 | 1.0 | 1.7 | ASW00096rm | 1.0 | A/R,R |
| SW44 | CFHTLS J020810-040220 | 32.0450 | -4.0389 | 1.0 | 20.8 | 1.8 | 1.3 | ASW0001c3j | 0.7 | A,R |
| SW45 | CFHTLS J021021-093415 | 32.5898 | -9.5711 | 0.4 | 18.4 | 2.7 | 1.3 | ASW0002k40 | 0.4 | D,S |
| SW46 | CFHTLS J021225-085211 | 33.1051 | -8.8697 | 0.8 | 19.5 | 2.1 | 1.3 | ASW00024id | 1.0 | R,R |
| SW47 | CFHTLS J021317-084819 | 33.3234 | -8.8055 | 0.5 | 19.8 | 1.3 | 1.3 | ASW00024q6 | 0.4 | A,R/E |
| SW48 | CFHTLS J022843-063316 | 37.1794 | -6.5547 | 0.5 | 19.1 | 1.8 | 1.3 | ASW0003r6c | 0.3 | D/A,E |
| SW49 | CFHTLS J090219-053923 | 135.5794 | -5.6566 | 0.0 | 0.0 | 2.0 | 1.3 | ASW0000g95 | 1.0 | A,R/E |
| SW40 | CFHTLS J090319-040146 | 135.8311 | -4.0297 | 0.0 | 19.8 | 1.2 | 1.3 | ASW00007ls | 0.5 | A,R/E |
| SW51 | CFHTLS J090333-005829 | 135.8886 | -0.9749 | 0.0 | 0.0 | 2.1 | 1.3 | ASW00008a0 | 1.0 | A/D,E/G |
| SW52 | CFHTLS J135724+561614 | 209.3536 | 56.2707 | 0.0 | 0.0 | 2.6 | 1.3 | ASW0006e0o | 0.9 | D,E |
| SW53 | CFHTLS J140027+541028 | 210.1164 | 54.1746 | 0.0 | 0.0 | 1.2 | 1.3 | ASW0006a07 | 0.6 | Q,R/E |
| SW54 | CFHTLS J140425+520506 | 211.1062 | 52.0850 | 0.4 | 18.9 | 1.4 | 1.3 | ASW0005o0w | 0.6 | D,E |
| SW55 | CFHTLS J141518+513915 | 213.8290 | 51.6542 | 0.4 | 18.3 | 3.0 | 1.3 | ASW00070vl | 0.8 | D,E |
| SW56 | CFHTLS J142620+561356 | 216.5870 | 56.2323 | 0.5 | 19.5 | 1.3 | 1.3 | ASW0007sez | 0.8 | A/R,S |
| SW57 | CFHTLS J142652+560002 | 216.7201 | 56.0006 | 0.0 | 0.0 | 1.5 | 1.3 | ASW0007t5y | 1.0 | R,R |
| SW58 | CFHTLS J142843+543713 | 217.1815 | 54.6204 | 0.4 | 19.7 | 1.3 | 1.3 | ASW0007pga | 0.6 | D,D |
| SW59 | CFHTLS J143631+571131 | 219.1315 | 57.1922 | 0.7 | 20.9 | 1.3 | 1.3 | ASW0008pag | 0.6 | D/A,R |
| SW60 | CFHTLS J143651+530705 | 219.2150 | 53.1183 | 0.6 | 19.2 | 3.1 | 1.3 | ASW0007h27 | 1.0 | A,E/G |
| SW61 | CFHTLS J143950+544606 | 219.9609 | 54.7686 | 0.0 | 0.0 | 1.7 | 1.3 | ASW00085cp | 0.4 | A,G/R |

The column Comments has two type of notes. The first is about the lens image configuration where the symbols mean the following A: Arc, D: Double, Q: Quad, R: Ring. The second is a comment on the type of lens assessed visually. Note that this classification is not based on colors or spectral analysis. The symbols are E: Elliptical, S: (face on) Spiral, G: Group-scale, D: Edge on disk, R: Red starforming galaxy. This galaxy falls within the masked region as per the catalog from which the magnitudes and the redshift are extracted.

**ACKNOWLEDGEMENTS**

We thank all XXXmembers of the Space Warps community for their contributions to the project so far. A complete list of collaborators is given at... In particular we would like to recognise the efforts of XXX, YYY etc in moderating the discussion.

We are also grateful to Brooke Simmons, David Hogg, XXX and YYY for many useful conversations about citizen science and gravitational lens detection. PJM was given support by the Royal Society, in the form of a research fellowship, and by the U.S. Department of Energy under contract number DE-AC02-76SF00515. AV acknowledges support from the Leverhulme Trust in the form of a research fellowship. The work of AM and SM was supported by World Premier International Research Center Initiative (WPI Initiative), MEXT, Japan. The work of AM was also supported in part by National Science Foundation Grant No. PHYS-1066293 and the hospitality of the Aspen Center for Physics. The Space Warps project is open source. The web app was developed at https://github.com/Zooniverse/Lens-Zoo while the SWAP analysis software was developed at https://github.com/drphilmarshall/SpaceWarps. This work is based on observations obtained with MegaPrime/MegaCam, a joint project of CFHT and CEA/IRFU, at the Canada-France-Hawaii Telescope (CFHT) which is operated by the National Research Council (NRC) of Canada, the Institut National des Sciences de l'Univers of the Centre National de la Recherche Scientifique (CNRS) of France, and the University of Hawaii. This research used the facilities of the Canadian Astronomy Data Centre operated by the National Research Council of Canada with the support of the Canadian Space Agency. CFHTLenS data processing was made possible thanks to significant computing support from the NSERC Research Tools and Instruments grant program.

**REFERENCES**

Bernardi, M., et al. 2003, AJ, 125, 1866
Chan, J. H. H., Suyu, S. H., Chiueh, T., More, A., Marshall, P. J., Coupon, J., Oguri, M., & Price, P. 2014, ArXiv e-prints
Coupon, J., et al. 2009, A&A, 500, 981
Erben, T., et al. 2013, MNRAS, 433, 2545
Faber, S. M., et al. 2007, ApJ, 665, 265
Faure, C., et al. 2009, ApJ, 695, 1233
Frei, Z., & Gunn, J. E. 1994, AJ, 108, 1476
Gavazzi, R., Marshall, P. J., Treu, T., & Sonnenfeld, A. 2014, ApJ, 785, 144
Gnedin, O. Y., Kravtsov, A. V., Klypin, A. A., & Nagai, D. 2004, ApJ, 616, 16
Hildebrandt, H., et al. 2012, MNRAS, 421, 2355
Keeton, C. R., Christlein, D., & Zabludoff, A. I. 2000, ApJ, 545, 129
Lintott, C. J., et al. 2008, MNRAS, 389, 1179
Lupton, R., Blanton, M. R., Fekete, G., Hogg, D. W., O'Mullane, W., Szalay, A., & Wherry, N. 2004, PASP, 116, 133
More, A., Cabanac, R., More, S., Alard, C., Limousin, M., Kneib, J.-P., Gavazzi, R., & Motta, V. 2012, ApJ, 749, 38
Navarro, J. F., Frenk, C. S., & White, S. D. M. 1997, ApJ, 490, 493
Oguri, M. 2006, MNRAS, 367, 1241
Oguri, M., & Marshall, P. J. 2010, MNRAS, 405, 2579
Pâris, I., et al. 2012, A&A, 548, A66
Parker, L. C., Hudson, M. J., Carlberg, R. G., & Hoekstra, H. 2005, ApJ, 634, 806
Richards, G. T., et al. 2006, AJ, 131, 2766
Schwamb, M. E., et al. 2012, ApJ, 754, 129
Sygnet, J. F., Tu, H., Fort, B., & Gavazzi, R. 2010, A&A, 517, A25

This paper has been typeset from a TEX/ LATEX file prepared by the author.